photonics

MDPI

Article

Fast Non-Mechanical Beam Steering via Cascaded Stressed Polymer Network Liquid Crystal Optical Switch and Liquid Crystal Polarization Grating

Jiahui Chen [1], Ziling Chen [1], Xitong Liang [1], Yuan Wang [1], Lin Xu [1,*] and Chi Zhang [2,*]

[1] School of Science, Jiangsu University of Science and Technology, Zhenjiang 212100, China; 232210505205@stu.just.edu.cn (J.C.); chenziling585@gmail.com (Z.C.); wangyuan@just.edu.cn (Y.W.)
[2] National Key Laboratory of Electromagnetic Space Security, Tianjin 300308, China
* Correspondence: xulin@just.edu.cn (L.X.); chi_zhang.94@foxmail.com (C.Z.)

Abstract

Non-mechanical beam steering technology based on liquid crystal optical switches and liquid crystal polarization gratings holds significant application prospects in fields such as laser communication, radar detection, and optical information processing. Traditional nematic liquid crystal optical switches exhibit slow response speeds, whereas novel ferroelectric liquid crystal optical switches, despite their fast response, are hampered in engineering applications by complex fabrication processes, the large number of devices required for cascading, and substantial module thickness. To address these issues, this paper proposes and demonstrates a fast non-mechanical beam steering scheme by cascading a stressed polymer network liquid crystal (SPNLC) optical switch with a liquid crystal polarization grating. The SPNLC is fabricated by mechanically shearing a polymerized liquid crystal–polymer composite, enabling sub-millisecond response and continuous linear phase modulation without the need for an alignment layer. A 30-μm-thick SPNLC half-wave plate was prepared, which introduces a phase retardation of 3.6 μm under a driving voltage of 300 V, and the rise time and fall time are measured to be approximately 526 μs and 560 μs at a driving voltage of 20 V with a 1 kHz square wave, and 470 μs and 538 μs at 27 V under the same waveform conditions. Cascaded with a passive polarization grating, the waveplate enables fast electrical switching of the beam between the ±1st diffraction orders. Furthermore, a two-dimensional multi-angle beam deflector was constructed based on a supra-binary cascade scheme. Experimental results confirm that the system possesses sub-millisecond response, large phase retardation, continuous tunability, and an alignment-layer-free fabrication process, demonstrating its feasibility for large-range fast beam scanning.

Keywords: stressed polymer network liquid crystal; fast response; phase modulation; beam steering; diffractive optics; polarization grating

Check for updates

Received: 11 July 2026
Revised: 20 August 2026
Accepted: 21 August 2026
Published: 23 August 2026

Copyright: © 2026 by the authors. Licensee MDPI, Basel, Switzerland. This article is an open access article distributed under the terms and conditions of the Creative Commons Attribution (CC BY) license.

1. Introduction

Non-mechanical beam steering technology is a core enabling component of modern electro-optical systems such as free-space optical communication, lidar, optical phased arrays, and adaptive optics [1,2]. As these fields impose increasingly stringent requirements on system integration, response speed, and beam manipulation flexibility, traditional mechanical steering schemes based on gimbals and rotating mirrors have gradually become

bottlenecks limiting further system performance improvement due to their inherent drawbacks, including bulky volume, high power consumption, response latency, and mechanical wear [3,4]. Consequently, the exploration of a solid-state beam steering solution featuring no moving parts, compact structure, rapid response, and high controllability has become a research frontier and urgent demand in the field of optoelectronic engineering.

Among various non-mechanical beam steering technologies, liquid crystal materials have attracted considerable attention due to their high birefringence, low power consumption, and mature fabrication processes. However, the response speed of conventional nematic liquid crystal devices is constrained by the square-law relationship between rotational viscosity and cell gap, and their millisecond-level response time falls short of the requirements for highly dynamic scenarios such as laser communication, radar scanning, and atmospheric turbulence compensation [5].

To overcome the aforementioned speed bottleneck, researchers have proposed overdrive technology [6] and driving architectures such as In-Plane Switching (IPS) and Vertical Alignment (VA) [7,8], and have explored various fast liquid crystal material systems and device designs. For example, Fan et al. used dual-frequency liquid crystals (DFLC) to fabricate a polymer gel-based optical switch, achieving an electrically controlled response time of less than one millisecond (~0.8 ms) [9]; Kowerdziej et al. further integrated DFLC with a nanoplasmonic metasurface and, through frequency switching, achieved electrical tuning of the resonance wavelength with a total response time of only 1.89 ms [10]; and Cattaneo et al. demonstrated an all-optical ultrafast modulation scheme based on the femtosecond laser-induced optical Kerr effect, with response times as low as 500 femtoseconds (fs) [11]. In addition, emerging material systems such as blue-phase liquid crystals [12,13] also show great application potential due to their sub-millisecond response times and the advantage of not requiring an alignment layer.

Among the many fast-response liquid crystal materials, ferroelectric liquid crystals (FLCs) have attracted particular attention due to their intrinsically microsecond-level electro-optic response arising from spontaneous polarization. Recently, Guo et al. [14] combined an FLC phase shutter with a passive polarization grating (PG), exploiting the bistable polarization switching of FLCs to achieve rapid beam steering between the ± 1 diffraction orders, with a switching time of 82 μs and a diffraction efficiency of 95.7% at 1064 nm. Subsequently, Yuan et al. [15] integrated an FLC half-wave plate with cascaded polarization gratings and a q-plate to realize fast optical vortex steering and high-speed encoding of 32 distinct orbital angular momentum states, with switching times below 70 μs. Yuan Fang et al. [16] combined an FLC half-wave plate with a two-stage cascaded liquid crystal polymer polarization grating to achieve 4-channel fast beam scanning over a large angle of 22.9°, with a response time below 70 μs and a system efficiency of 86.3%. These works fully demonstrate the unparalleled superior performance of FLCs in high-speed polarization control. However, the phase modulation mode of FLC devices is intrinsically constrained by their surface-stabilized bistable (or limited grayscale) states, lacking continuous analog control over phase retardation. Meanwhile, achieving high-quality FLC alignment relies heavily on precise photo-alignment techniques using photosensitive azo-dyes such as SD1, a process that is complex and demanding in terms of environmental cleanliness. On the other hand, FLC-based cascaded beam steering schemes typically require multiple devices to work together. Each FLC half-wave plate must be paired with two quarter-wave plates (QWPs) and cascaded with a liquid crystal polarization grating (LCPG), resulting in at least four devices per single deflection module. Such a multi-layer stack significantly increases the module thickness and presents challenges for compact system integration and practical engineering applications.

To address the technical gap of the aforementioned FLC schemes, stressed polymer network liquid crystals (SPNLCs) offer a fundamentally distinct physical pathway. As illustrated in Figure 1, SPNLCs are derived from conventional polymer network liquid crystals (PNLCs), with the core innovation being the application of mechanical shear stress to the polymerized liquid crystal–polymer composite film. In the as-polymerized PNLC, the liquid crystal microdomains are randomly oriented, rendering the device strongly scattering (Figure 1a). Upon application of shear stress, the polymer network is stretched and oriented along the shearing direction, inducing unidirectional alignment of the liquid crystal microdomains and transitioning the device from the scattering state to the transparent state (Figure 1b). This stretched and oriented polymer network provides a rapid elastic restoring force to the liquid crystal molecules after the electric field is removed, enabling SPNLCs to maintain sub-millisecond response while achieving effective decoupling of response speed from cell thickness. That is, when the cell thickness is increased to obtain larger phase retardation, the response time no longer follows the square-law degradation characteristic of conventional nematic liquid crystals (Figure 1c) [17,18].

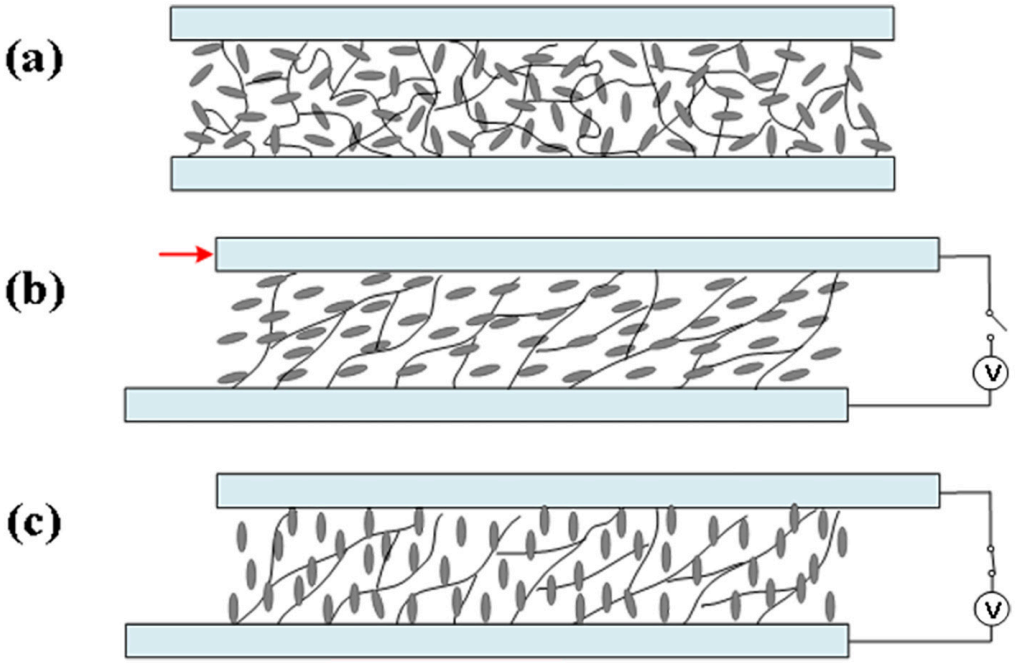


Figure 1. Schematic diagram of the SPNLC cell. (**a**) After polymerization; (**b**) after shearing (the red arrow indicates the direction of shearing); (**c**) after electric field application.

On the other hand, liquid crystal polarization gratings (LCPGs), as typical liquid crystal geometric phase optical elements, exhibit rigorous polarization-selective diffraction characteristics, with a theoretical single-order diffraction efficiency of up to 100%. Cascading multiple LCPGs enables large-range multi-angle beam coverage [19–21]. However, LCPGs are passive components whose deflection directions are permanently fixed, necessitating a high-speed switchable polarization state controller in front of them to achieve electrically controlled dynamic deflection.

Based on the above analysis, we propose and demonstrate a novel beam deflector scheme that integrates the fast polarization control capability of SPNLCs with the high-efficiency polarization-selective diffraction characteristics of LCPGs. The core architecture is as follows: a shear-fabricated SPNLC electrically tunable half-wave plate serves as the front-end polarization switch, leveraging its linear voltage response to achieve fast switching of the incident circular polarization handedness, thereby determining the beam deflection direction after passing through the LCPG; a two-dimensional large-angle multi-

state deflection module is then constructed via an orthogonal supra-binary cascade scheme. The dynamic response performance of the unit module was characterized: at 20 V and 1 kHz square-wave excitation, the rise and fall times of the 30-μm-thick SPNLC were measured as 526 μs and 560 μs, while at 27 V they were 470 μs and 538 μs, respectively; under a 300 V high-voltage drive, the device introduces a phase retardation of 3.6 μm, demonstrating a relatively wide linear phase modulation range (30–90 V). The SPNLC device in this work achieves sub-millisecond response speed, provides continuous linear phase modulation capability, and delivers a large phase retardation up to several micrometers. In addition, its fabrication process requires no alignment layer, significantly simplifying device preparation and reducing environmental sensitivity. These inherent advantages make the SPNLC a promising candidate for applications requiring fast response, large phase depth, and fabrication simplicity.

2. Materials and Methods

2.1. Fabrication of SPNLC

The fabrication of the SPNLC waveplate mainly followed the method reported in Ref. [18], but with an additional low-temperature polymerization treatment introduced in our process. The conventional procedure consists of four steps: material preparation, cell assembly, UV polymerization, and stress shearing, as illustrated in Figure 2.

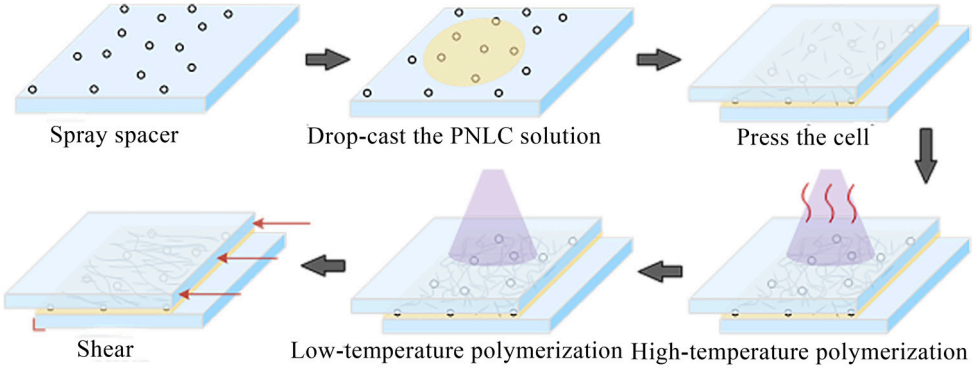


Figure 2. Schematic illustration of the SPNLC waveplate fabrication process (the red arrow indicates the direction of shearing).

First, in the PNLC solution preparation stage, the nematic liquid crystal 5CB (Aladdin, Shanghai, China), the reactive monomer RM82 (Aladdin, Shanghai, China), and the photopolymer NOA65 (Aladdin, Shanghai, China) were mixed at a weight ratio of 90:2:8, with 0.2 wt% photoinitiator BDK (Aladdin, Shanghai, China) additionally added. The mixture was then placed on a hotplate for heat treatment at 90 °C and stirred magnetically using a rotor until a homogeneous liquid crystal–monomer composite solution was formed. Finally, the PNLC solution was placed in a vacuum chamber for degassing.

In the cell assembly stage, to ensure uniformity of the cell gap, the ITO-coated glass substrates (Yingkou OPV Tech New Energy Co., Ltd., Yingkou, China) were first rigorously cleaned, and surface dust and contaminants were removed by high-pressure air blowing. Subsequently, spherical spacers with a diameter of 30 μm were uniformly sprayed onto the substrate surface to precisely control the cell gap. A single-end-sealed capillary tube was then used to draw an appropriate amount of the PNLC solution and introduce it into the effective electrode area of the bottom substrate. The top substrate was then precisely aligned and laminated against the bottom substrate with its ITO side facing inward; the lamination process was carried out as slowly as possible to prevent the formation of air

bubbles. Finally, the top substrate of the cell was gently pressed and slid to allow the PNLC solution to fill the entire cell and ensure a uniform cell gap.

The UV photopolymerization step was divided into two stages: high-temperature polymerization and low-temperature polymerization. First, the cell was placed on a hotplate at 90 °C and exposed to UV light at 365 nm (UVGO-365nm, Zhongshan Miaogu Lighting Co., Ltd., Zhongshan, China) with an intensity of 30 mW/cm^2 for 80 min. During this stage, the liquid crystal mixture was in the isotropic state, and the elevated temperature significantly reduced the system viscosity, accelerating the diffusion and crosslinking of the RM82 monomer, which increased the crosslinking density of the polymer network and reduced the domain size. The hotplate temperature was then lowered to room temperature (25 °C), and the cell was exposed to UV light for an additional 20 min to ensure complete polymerization of the monomers. Figure 3a shows the as-polymerized PNLC sample in a strongly scattering state. After these two consecutive polymerization stages, the device could be rendered highly transparent through stress shearing. The shearing force propagated through the network structure among the liquid crystal molecules, enabling them to overcome local constraints and become uniformly aligned along the shearing direction.

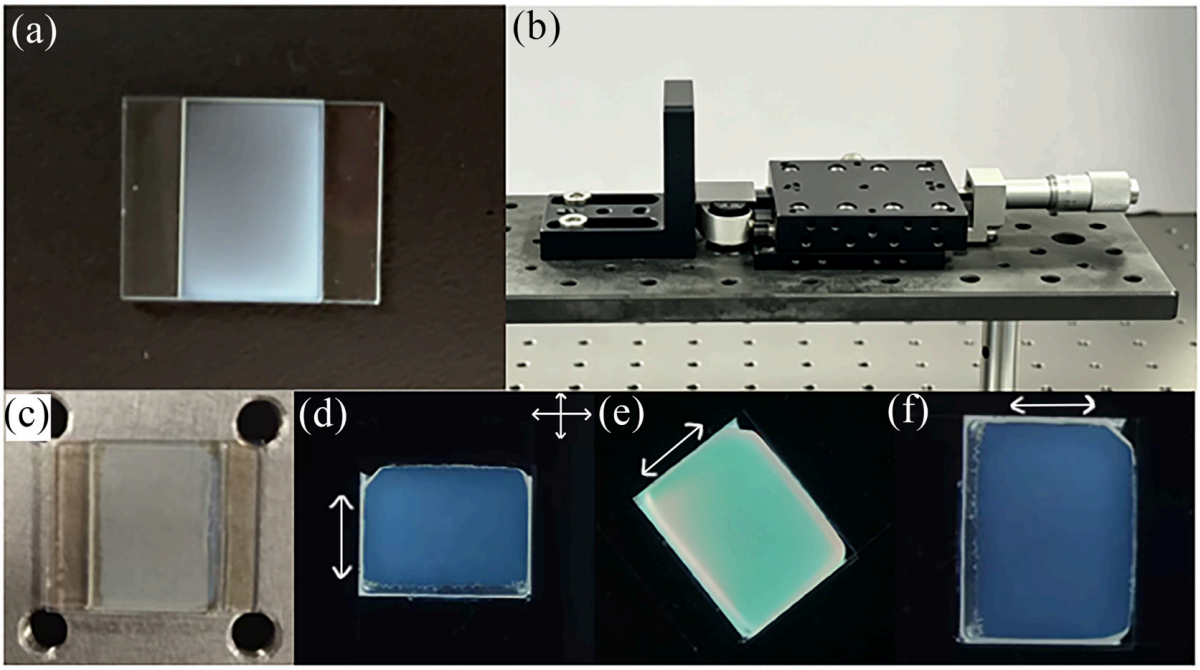


Figure 3. (**a**) The as-polymerized PNLC sample. (**b**) Photograph of the shearing apparatus for SPNLC fabrication. (**c**) Photograph of the fabricated SPNLC waveplate; (**d**–**f**) appearance of the SPNLC waveplate at different azimuthal angles between crossed polarizers. The white arrows next to the devices in Figures (**d**–**f**) indicate the direction of shear; the arrow in the upper-right corner of Figure (**d**) indicates the orientation of the orthogonal polarizer.

Figure 3b shows a photograph of the shearing apparatus. Its core components are the stop plate on the left, the precision translation stage on the right (whose displacement is controlled by a screw micrometer), and the glass stage in the centre on which the liquid crystal cell is placed. The screw micrometer must be moved by 10 μm. During operation, the bottom substrate of the cell was positioned against the left stopper plate, and the micrometer was slowly rotated until the edge of the translation stage was tightly pressed against the edge of the top substrate of the cell. Before shearing, the SPNLC cell was in a strongly scattering state. As shearing began, the haze of the cell gradually decreased, and the liquid crystal layer became increasingly transparent, indicating that the liquid crystal molecules were becoming aligned along the shearing direction, with their long axes

oriented parallel to the shearing direction. The shearing process was completed when the transmittance of the cell reached its maximum. If the shearing distance was excessive, the network structure within the liquid crystal layer could be fractured. Therefore, the displacement per shearing step was kept as small as possible throughout the process.

After shearing was completed, the edges of the liquid crystal cell were sealed and fixed with UV adhesive. The UV adhesive required thorough curing; otherwise, the stretched network structure inside the SPNLC would relax back. After the sealing process was finished, the SPNLC waveplate was successfully fabricated. Figure 3c shows a photograph of the fabricated SPNLC waveplate in this study. Compared with the strongly scattering state shown in Figure 3a, the haze of the SPNLC waveplate was significantly reduced after shearing. As shown in Figure 3d–f, when the SPNLC waveplate sample was placed between crossed polarizers and its azimuthal angle was rotated, alternating bright and dark transmitted intensity was observed in the active area of the sample.

In contrast to the SPNLC waveplate preparation method used in Ref. [18], the major difference in the present work lies in the implementation of a two-step polymerization scheme, namely, high-temperature polymerization followed by low-temperature polymerization. Moreover, the 405 nm working wavelength is approximately one-quarter of the 1550 nm wavelength, which is the direct cause of the particularly prominent scattering effect observed later. A comprehensive comparison of the fabrication processes and critical performance parameters of the SPNLC waveplates is given in Table 1.

Table 1. Comparison of fabrication processes and key performance parameters of SPNLC waveplates between this study and Ref. [18].

Parameter	Wang et al. (2005) [18]	This Work
Cell thickness	40 μm	30 μm
UV curing conditions	50 °C, 20 mW/cm^2, 60 min (single step)	90 °C, 30 mW/cm^2, 80 min + 25 °C, 30 mW/cm^2, 20 min (two steps)
Shearing distance	80 μm	10 μm
Operating wavelength	1550 nm (near-infrared)	405 nm (visible)
Phase retardation	3.1 μm (reflective mode, equivalent)	3.6 μm (transmissive mode, at 300 V)
Response time (rise/fall)	55 μs/30 μs (at 200 V)	470 μs/538 μs (at 27 V)
Linear range of the drive voltage	67–191 V	30–90 V
Application scenario	Optical phased array (wavefront correction)	Fast beam steering with SPNLC + LCPG

2.2. LCPG Fabrication

Liquid crystal polarization gratings (LCPGs) are typically fabricated by combining polarization holography and photoalignment techniques. In this work, the LCPGs were prepared using circular polarization holographic exposure [22,23], with three configurations employed for grating orientation: a Mach–Zehnder interferometer, a conventional two-beam interference setup, and a template shearing interferometry method. These approaches share the same physical principle: by precisely controlling the incidence angle between two coherent circularly polarized beams through an optical system, a spatially continuously varying polarization field is induced on the SD1 alignment layer.

The fabrication process of LCPGs is schematically illustrated in Figure 4. First, the photoalignment material SD1 (Nanjing Jingcui Optics Technology Co., Ltd., Nanjing, China) solution was spin-coated onto thoroughly cleaned glass substrates with a spin-coating program of 600 rpm for 6 s, followed by acceleration to 3000 rpm for 30 s. After spin-coating, the substrates were baked on a hotplate at 100 °C for 15 min to remove residual solvent and

cure the alignment layer. Subsequently, holographic exposure was performed using a 457 nm laser (MSL-U-457-100 mW, CNI, Qingdao, China) as the light source, with the exposure dose precisely controlled within 3–5 J/cm^2. During this process, SD1 molecules aligned perpendicular to the polarization direction of the electric field through photoisomerization, forming a periodic alignment pattern. The liquid crystal (LC) Polymer solution was prepared by dissolving 96 wt% polymerizable liquid crystal monomer RM257(Aladdin, Shanghai, China) and 4 wt% photoinitiator BDK as solutes in toluene at a solid content of 10 wt%. The prepared LC Polymer solution was then spin-coated onto the alignment layer using the same spin-coating program (600 rpm for 6 s, followed by 3000 rpm for 30 s). During spin-coating, the liquid crystal molecules aligned along the SD1-induced orientation direction. Subsequently, UV polymerization was carried out at 365 nm under a nitrogen-rich atmosphere to cure the film. The thickness of each LC Polymer layer depended on the RM257 solution concentration and the spin-coating parameters. By repeating the spin-coating and curing steps, the film thickness was gradually increased until the total thickness satisfied the half-wave condition ($\Delta n_1 d_1 = \lambda/2$, where Δn_1 is the birefringence of the RM257 material, d_1 is the LCPG film thickness, and $\lambda = 405$ nm), thereby completing the fabrication of LCPGs with high diffraction efficiency.

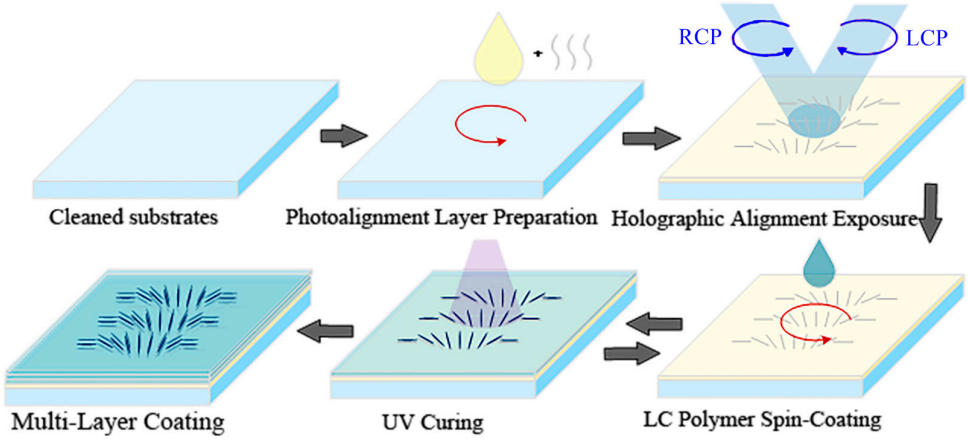


Figure 4. Schematic diagram of the LCPG fabrication process flow; in the figure, the red arrows indicate the spin-coating process, whilst the blue arrows represent right-handed circularly polarized (RCP) light and left-handed circularly polarized (LCP) light, respectively.

Figure 5 shows a photograph of the LCPG sample fabricated in our laboratory and its diffraction pattern under broadband white light illumination. The intrinsic diffraction efficiency of the as-fabricated LCPG was measured to be 97%.

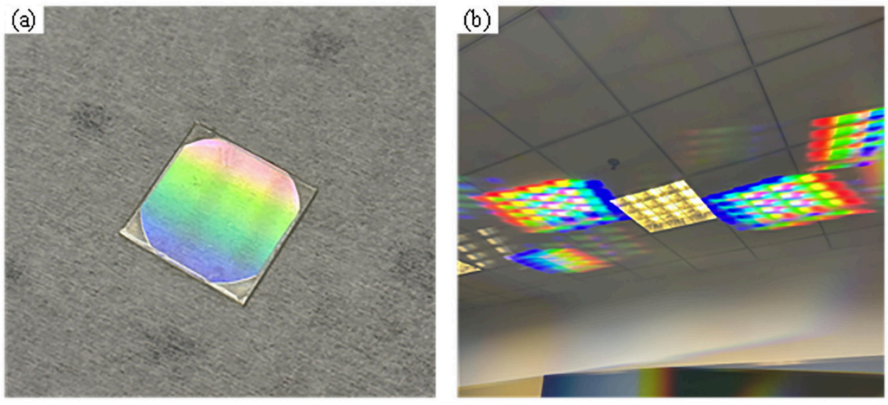


Figure 5. (**a**) Photograph of the as-fabricated LCPG sample; (**b**) diffraction pattern of the LCPG under white light illumination.

2.3. Experimental Methods

In terms of diffraction characteristics, LCPGs exhibit pronounced polarization sensitivity governed by the polarization-selective diffraction rule. When left-handed circularly polarized (LCP) light is incident, the transmitted beam is converted into right-handed circularly polarized (RCP) light with its energy concentrated in the +1st diffraction order. Conversely, when RCP light is incident, the transmitted beam is converted into LCP light with its energy concentrated in the −1st diffraction order. In this process, the handedness of the circularly polarized light is reversed upon transmission, which is a characteristic signature of the liquid crystal geometric phase effect. For incident linearly or elliptically polarized light, which can be decomposed into a superposition of LCP and RCP components with different proportions, the two circular components are diffracted into the +1st and −1st orders, respectively. By adjusting the polarization state of the incident light, the energy distribution between the two diffraction orders can be precisely controlled, enabling flexible manipulation of the intensity distribution.

LCPGs convert the handedness information of incident circularly polarized light into spatial deflection direction—left-handed circular polarization corresponds to the +1st order and right-handed to the −1st order, with the handedness of the transmitted beam automatically reversed. Based on this property, electrical switching of the beam deflection direction can be achieved by placing the SPNLC electrically tunable waveplate in front of the LCPG to switch the handedness of the incident circular polarization.

In 2011, Kim et al. from North Carolina State University systematically analyzed several LCPG cascade schemes in terms of key performance metrics such as transmittance loss, number of deflection angles, and deflection range [21]. The supra-binary cascade scheme enables a larger beam deflection range while using fewer LC cells. By orthogonally cascading two LCPG modules, a two-dimensional large-range multi-angle beam deflection module can be constructed.

In summary, the experimental scheme of this study consists of three sequential steps. First, the voltage-tunable phase modulation capability of the SPNLC waveplate is verified by measuring the voltage–phase retardation curve. Second, an elementary module composed of a single SPNLC waveplate and a single LCPG is assembled to observe the beam deflection between the ±1st diffraction orders, and the switching response time is measured to characterize its fast response capability. Third, a two-dimensional cascaded module based on the supra-binary scheme is constructed to demonstrate beam deflection in four distinct directions. The measurement results of the above experiments are presented in the following sections.

3. Results

3.1. Voltage–Phase Retardation Characteristics of SPNLC

The SPNLC waveplate exhibits continuous phase modulation capability. As shown in Figure 6, the waveplate was placed between crossed polarizers with its azimuthal angle set to 45°. AC driving voltages of 20 V, 40 V, 60 V, 80 V, 120 V, and 200 V were applied sequentially. With increasing driving voltage amplitude, the SPNLC waveplate introduced different phase retardations, as evidenced by the varying transmitted intensities. When the driving voltage reached 200 V, the LC molecules within the cell were vertically aligned, and a small region of the sample appeared dark.

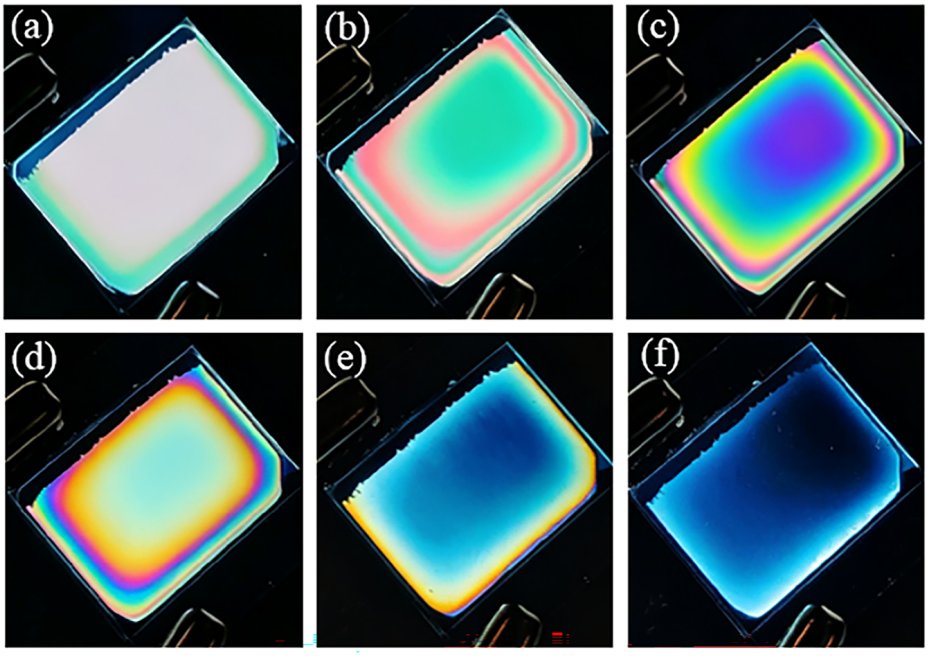


Figure 6. Polarized optical micrographs of the SPNLC waveplate under different driving voltages in crossed polarizers. (**a**) 20 V; (**b**) 40 V; (**c**) 60 V; (**d**) 80 V; (**e**) 120 V; (**f**) 200 V.

To verify the continuous phase modulation capability of the SPNLC under high-voltage driving, we constructed the phase retardation measurement setup shown in Figure 7 based on the quarter-wave plate method [24,25]. A 405 nm laser served as the light source. The optical axes of the polarizer and analyzer were set at 45° and 135° to the horizontal, respectively. A quarter-wave plate (QWP) was placed before the analyzer, with its optical axis aligned with that of the polarizer. The SPNLC sample under test was positioned between the QWP and the polarizer, with its fast and slow axes oriented at 45° to the transmission axis of the polarizer. A voltage amplifier was used to amplify the signal from a function generator to provide high-voltage driving to the SPNLC, enabling the device to introduce corresponding phase retardation to the incident light.

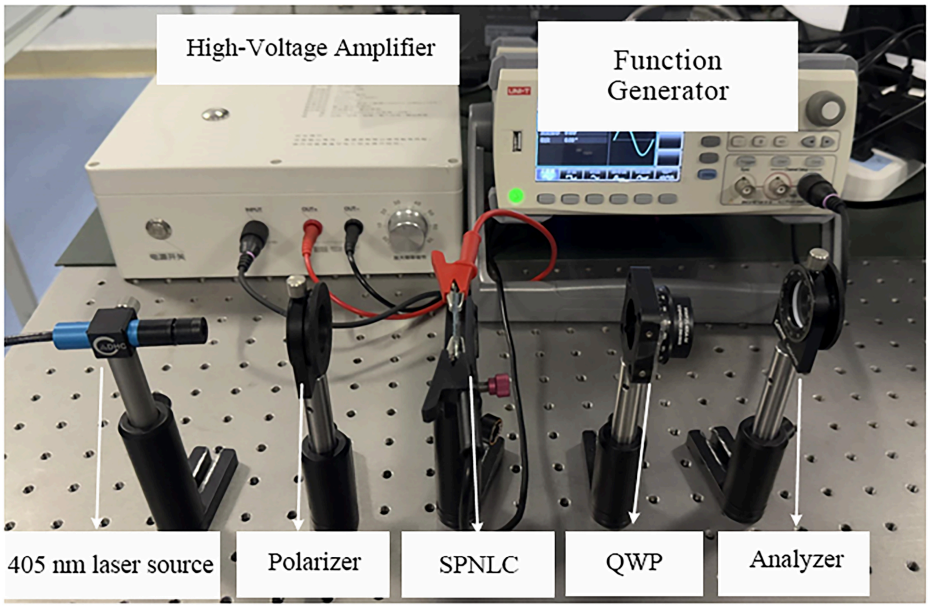


Figure 7. Photograph of the experimental setup for measuring the voltage–phase retardation curve of the SPNLC.

To measure the phase retardation, a voltage was applied to the SPNLC, and the analyzer was rotated until the transmitted light reached the dark state. The phase retardation was then determined from the rotation angle of the analyzer. By applying different driving voltages and recording the corresponding phase retardations, the voltage–phase retardation curve was obtained, as shown in Figure 8. The measured SPNLC sample had a cell gap of 30 μm. Under a driving voltage of up to 300 V, the device introduced a phase retardation of up to 3.6 μm, demonstrating a wide-range continuous phase modulation capability with a relatively broad linear modulation range. The voltage–phase retardation relationship was linearly fitted in the 30–90 V range as $\Delta OPD = -0.03574\ \mathrm{V} + 4.4061$, where ΔOPD (=$\Delta n_2 d_2$, with Δn_2 being the birefringence of the liquid crystal material and d_2 the cell gap) denotes the phase shift, and V is the applied voltage. The coefficient of determination R^2 was calculated to be 0.9932, confirming the excellent linearity of the phase modulation in this range.

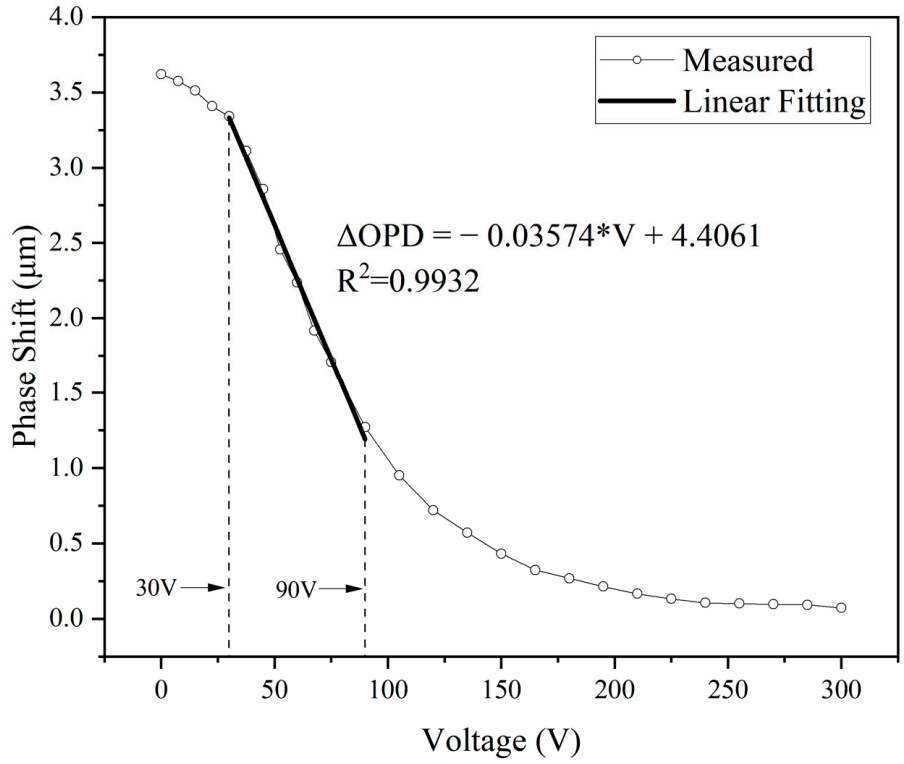


Figure 8. Measured voltage–phase retardation curve of the SPNLC. The linear modulation range is approximately 30–90 V.

3.2. Dynamic Response Characterization of the SPNLC-LCPG Module

Figure 9a presents the experimental setup for measuring the beam deflection performance of the LCPG based on the SPNLC waveplate. A 405 nm laser was used as the light source. The beam passed through a polarizer and was modulated into linearly polarized light. When the optical axis of the SPNLC was set at 45° to the incident linear polarization direction, AC voltages of different amplitudes (20 V and 27 V) were applied to the SPNLC waveplate to switch the output between right-handed and left-handed circularly polarized light. The resulting circularly polarized beam was then incident on the LCPG and diffracted to the ±1st orders, respectively. Figure 9b,c show the results of the beam deflection tests. It can be seen that the beam can be deflected by ±1 order, with a deflection efficiency of approximately 90 per cent.

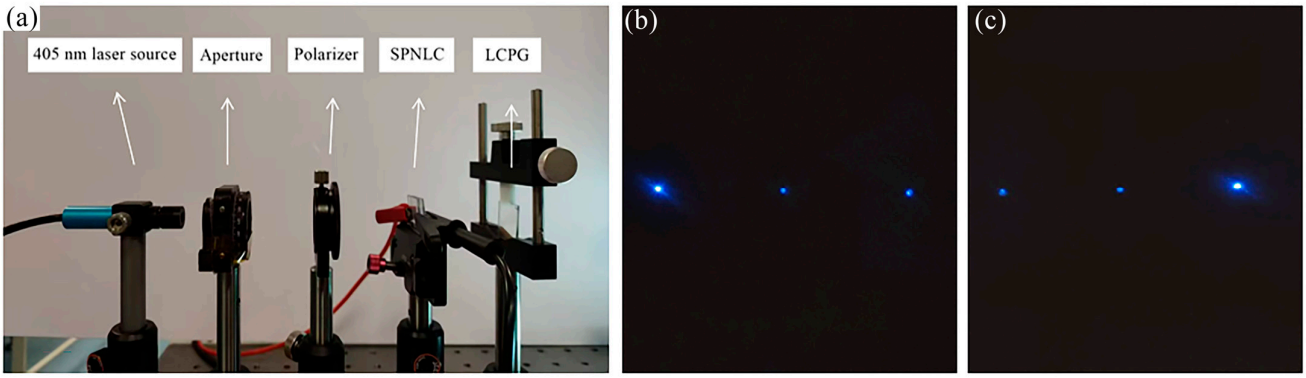


Figure 9. (**a**) Photograph of the experimental setup for beam deflection measurement of the LCPG based on the SPNLC waveplate; (**b**) beam steered to the −1st diffraction order; (**c**) beam steered to the +1st diffraction order.

To characterize the response time of the Liquid Crystal Waveplate (LCWP) within the LCPG module, a photodetector was used, and the experimental setup is shown in Figure 10. After the setup was prepared, the laser was turned on, and one of the output beams at a specific angle was aligned with the sensing head of the photodetector. A driving signal was applied to the electrically controllable waveplate in the LCPG module, causing the beam to switch periodically between the detection angle and its adjacent angle. The optical intensity variation detected by the photodetector was converted into an electrical signal, which appeared as alternating high- and low-level waveforms on an oscilloscope. The time required for the signal to rise from 10% to 90% of the maximum amplitude during the low-to-high transition was defined as the rise time (τ_{on}), and the time required for the signal to fall from 90% to 10% during the high-to-low transition was defined as the fall time (τ_{off}). In the characterization of liquid crystal devices, both τ_{on} and τ_{off} are collectively considered as the response time of the device.

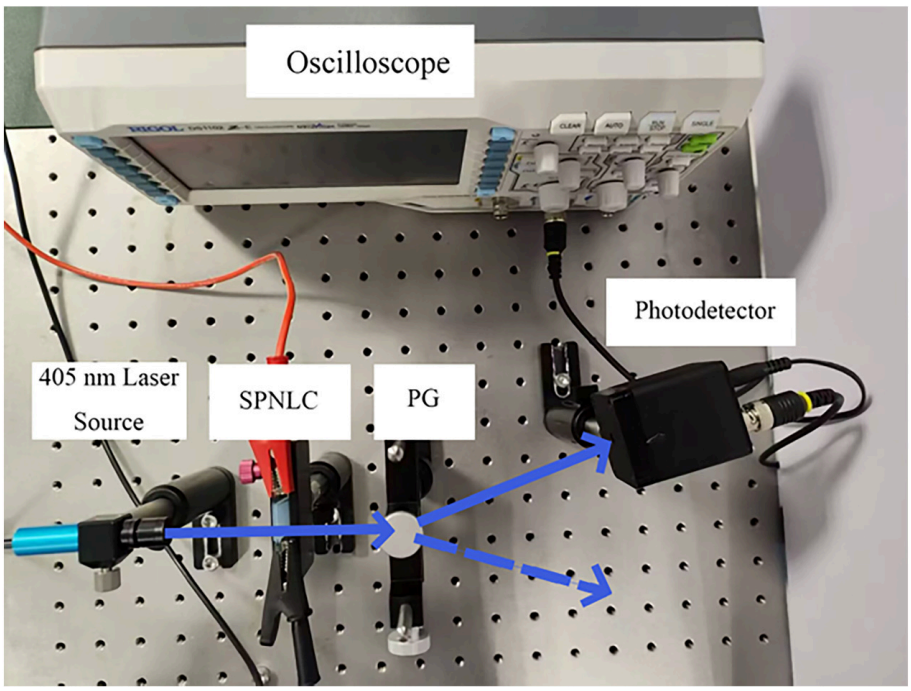


Figure 10. Photograph of the experimental setup for response time measurement of the SPNLC-LCPG module (the blue arrow indicates the direction of travel of the 405 nm laser beam).

The SPNLC under test has a cell thickness of 30 μm; drive voltages of 20 V and 27 V, applied as 1 kHz square-wave AC voltages, were used. The 20 V voltage corresponds to a λ/4 phase delay condition, whilst the 27 V voltage corresponds to a 3λ/4 phase delay condition—these two operating voltages represent the key states for the SPNLC to achieve circular polarisation rotation switching within the LCPG system. The test results for the drive voltage waveforms and response times are shown in Figure 11, where the vertical axis of the response time test results has been normalised. At a working voltage of 20 V, the rise-time response was approximately 526 μs and the fall-time delay was approximately 560 μs; at a working voltage of 27 V, the rise-time response was approximately 470 μs and the fall-time delay was approximately 538 μs, with response times reaching the sub-millisecond range. It is worth noting that sub-millisecond response times can be achieved with a low-voltage drive of just 20–27 V, demonstrating the SPNLC's advantage of rapid response under a low-voltage drive. If high-frequency switching is performed between two high-voltage levels, beam deflection with even faster response times can be achieved. Currently, due to limitations in laboratory equipment, it is not yet possible to achieve direct, rapid switching between 20 V and 27 V; consequently, the response times mentioned above were measured independently under on–off switching conditions at 0–20 V and 0–27 V, respectively. Nevertheless, both sets of data confirm that SPNLC possesses sub-millisecond response capabilities at the relevant operating voltages, with response speeds being of the same order of magnitude. In future work, we will further refine the experimental conditions to achieve direct switching between the two operating voltages, thereby enabling a more precise characterisation of the SPNLC's actual operational performance within the LCPG system.

3.3. Experiments on Beam Deflection in a Two-Dimensional Cascaded Module

The beam deflection test setup for the two-dimensional cascaded module is shown in Figure 12a. The optical path is formed by a cascade of components arranged in sequence along the optical axis, comprising a 405 nm laser source, an aperture, a polariser, the first SPNLC ($SPNLC_1$), the first liquid crystal polarising grating ($LCPG_1$), the second SPNLC ($SPNLC_2$) and the second LCPG ($LCPG_2$). To minimise the system's volume, the two LCPGs are arranged orthogonally in space and mounted on either side of $SPNLC_2$, forming a compact cascaded unit. To prevent high-voltage short circuits, the first SPNLC ($SPNLC_1$) is housed separately.

In the experiment, a 405 nm laser beam, after being confined by an aperture and passing through a polariser, is modulated into high-purity linearly polarised light. By adjusting the incident polarisation direction to form a 45° angle with the optical axis of $SPNLC_1$, the incident linearly polarised light is converted into circularly polarised light. By applying AC voltages of varying amplitudes to $SPNLC_1$, it functions as a waveplate with different delay values (λ/4 or 3λ/4), thereby switching the linearly polarised light to either right-handed or left-handed circularly polarised light. This circularly polarised light undergoes a first-order diffraction deflection in the horizontal direction after passing through $LCPG_1$; as the LCPG simultaneously reverses the circular polarisation hand during the diffraction process, the hand must be re-adjusted by $SPNLC_2$. By independently applying specific drive voltages to $SPNLC_2$, it selectively performs either 'polarisation reversal' or 'polarisation preservation' on the incident circularly polarised light; in conjunction with the orthogonally positioned $LCPG_2$, this enables deflection control in the vertical dimension. In the specific experiment, by applying four different combinations of alternating voltages (namely 20 V/20 V, 20 V/27 V, 27 V/27 V and 27 V/20 V) to the two SPNLC waveplates, respectively, the beam can be deflected to four different two-dimensional directions. Figure 12b–e shows the results of the beam deflection tests, where (b) corresponds to the drive voltage combination

of 20 V/20 V, (c) to 20 V/27 V, (d) to 27 V/27 V, and (e) to 27 V/20 V. It can be seen that, through the programmable combination of the two optical switches, the incident laser beam can be deflected to four different two-dimensional directions respectively. This thereby verifies the feasibility of the 'SPNLC + PG' technical architecture for rapid, non-mechanical, programmable beam deflection control.

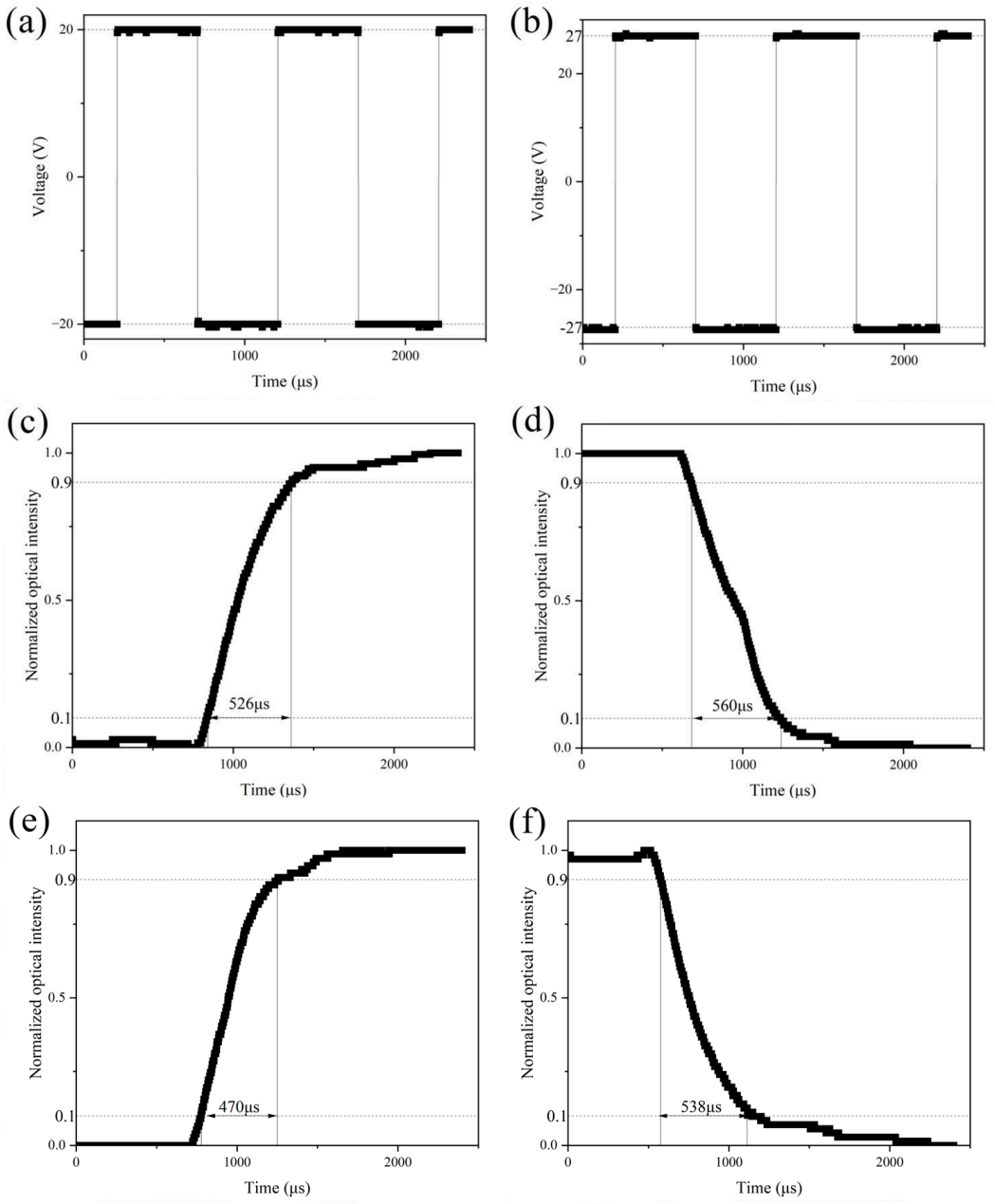


Figure 11. SPNLC response time test results for 20 V at 1 kHz and 27 V at 1 kHz. (**a**) Drive voltage waveform at 20 V, 1 kHz and 50% duty cycle. (**b**) Drive voltage waveform at 27 V, 1 kHz, and 50% duty cycle. (**c**,**d**) Rising-edge and falling-edge waveforms of the SPNLC response driven by 20 V. (**e**,**f**) Rising-edge and falling-edge waveforms of the SPNLC response driven by 27 V.

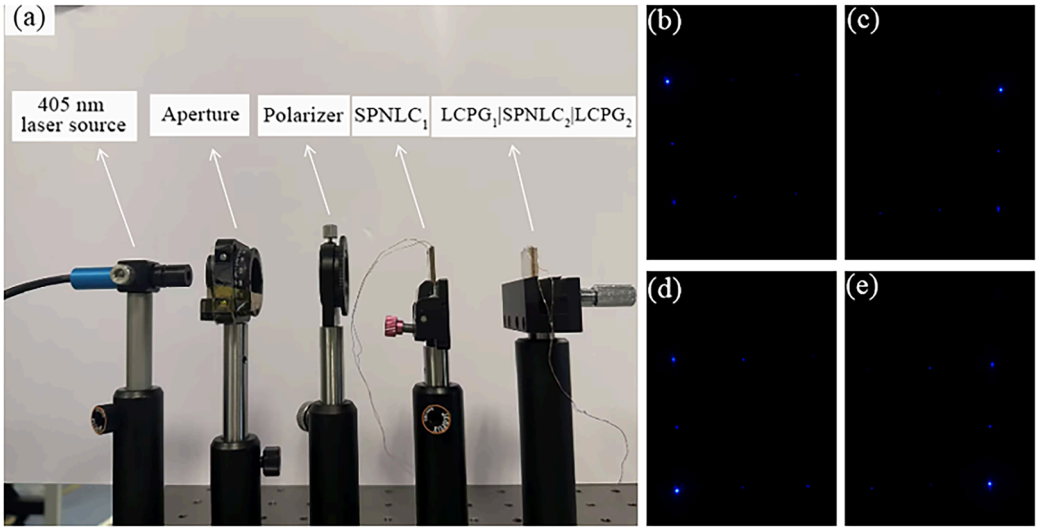


Figure 12. (**a**) Beam deflection test setup for a two-dimensional cascaded module. (**b**–**e**) Illustrations of beam deflection in four different directions. Specifically, the drive voltage combination in (**b**) is 20 V/20 V, in (**c**) it is 20 V/27 V, in (**d**) it is 27 V/27 V, and in (**e**) it is 27 V/20 V.

4. Discussion

In this work, fast non-mechanical beam steering was achieved by cascading a stressed polymer network liquid crystal optical switch with a liquid crystal polarization grating. The fast response and large phase retardation of the SPNLC can be attributed to its unique polymer network structure. The shear stress orients the polymer network along the stretching direction, providing a strong elastic restoring force to the liquid crystal molecules after the electric field is removed, thereby enabling a 30-μm-thick device to maintain sub-millisecond response. This observation confirms the decoupling of response speed from cell thickness in SPNLCs. In terms of phase modulation, the device introduces a phase retardation of 3.6 μm within 300 V and exhibits good linearity over the range of 30–90 V, satisfying the requirements for continuous wavefront control.

We analysed the relationship between response time, drive voltage and cell thickness based on the electro-optical model of SPNLC devices [26].

Relaxation time τ_{off}:

$$\tau_{\text{off}} = \frac{\gamma a^2}{K(l^2-1)} = \frac{\gamma R^2 l}{K(l^2-1)} \tag{1}$$

where γ is the rotational viscosity of the liquid crystal, R denotes the radius of the original spherical droplet, a is the major axis of the liquid crystal microdroplet, K is the bending elastic constant K_{33} of the liquid crystal, and the aspect ratio $l = \left(\frac{L}{d}\right)^2 + 1$, where L is the shear distance and d is the cell thickness.

Rise time (τ_{on}):

$$\tau_{on} = \frac{\gamma}{\sqrt{\left(\frac{K_{33}(l^2-1)}{R^2 l} + \Delta\varepsilon E^2\right)^2 + \left(\frac{K_{33}(l^2-1)}{R^2 l}\right) \cdot (\Delta\varepsilon E^2) \cdot \left(\frac{4}{l} - 4\right)}} \tag{2}$$

where $\Delta\varepsilon$ is the dielectric anisotropy of the liquid crystal, and E is the strength of the applied electric field.

Switching field (E_{switch}):

$$E_{\text{switch}} = \frac{V_{\text{switch}}}{d} = \frac{1}{3a}\left(\frac{\sigma_2}{\sigma_1} + 2\right)\left(\frac{K_{33}(l^2-1)}{\Delta\varepsilon}\right)^{\frac{1}{2}} = \frac{1}{3Rl}\left(\frac{\sigma_2}{\sigma_1} + 2\right)\left(\frac{K_{33}(l^2-1)}{\Delta\varepsilon}\right)^{\frac{1}{2}} \tag{3}$$

where σ_1 and σ_2 represent the electrical conductivities of the polymer matrix and the liquid crystal, respectively.

These three physical quantities are key parameters for assessing the electro-optical performance of SLC devices. Of these, the switching field $E_{\text{switch}} = \frac{V_{\text{switch}}}{d}$, where V_{switch} is the switching voltage defined as the voltage at which 90 per cent of the total optical path difference that the SLC cell is capable of providing is switched, and d is the thickness of the liquid crystal cell.

It can be seen from the relaxation time Equation (1) and the rise time Equation (2) that the response speed of the SPNLC is determined by the geometric dimensions of the liquid crystal microdroplets (major axis a, aspect ratio l) and the material parameters (rotational viscosity γ, elastic constant K) and has no direct functional relationship with the cell thickness d. Although the definition of the aspect ratio includes the shear distance L, L and d are independent process parameters; therefore, changing the cell thickness does not significantly affect the response time. Experimentally, a 30 μm device achieved rise/fall times of 526 μs/560 μs and 470 μs/538 μs under 20 V and 27 V drive voltages, respectively, confirming the maintainability of sub-millisecond response times under thick-cell conditions, which stands in stark contrast to the $\tau \propto d^2$ relationship observed in conventional liquid crystals. With regard to the drive voltage, it follows from the switching field Equation (3) that E_{switch} is determined by the droplet parameters and the material's electrical conductivity and is independent of the cell thickness d. Consequently, the drive voltage $V_{switch} = E_{\text{switch}} \cdot d$ is linearly proportional to the cell thickness—this is the physical trade-off required to achieve large phase delays using a thick-cell configuration.

Compared with the recently reported FLC-based beam steering schemes [12–14], the SPNLC achieves analog phase modulation by continuously tuning the tilt angle of liquid crystal molecules via the electric field to modify the effective refractive index, whereas FLC relies on the coupling between spontaneous polarization and the electric field for bistable switching, resulting in discrete binary or limited-grayscale phase modulation. In addition, the SPNLC requires only mechanical shearing for molecular alignment, eliminating the need for complex photo-alignment processes using SD1. From a system integration perspective, FLC-based cascaded schemes typically require multiple devices per deflection module. Each FLC half-wave plate must be paired with two quarter-wave plates and one LCPG, which leads to increased module thickness and fabrication complexity and consequently restricts their engineering applicability. In contrast, our SPNLC-based approach offers a substantially simplified system architecture. We conducted a systematic comparison of the two approaches based on key performance parameters, and the results are summarized in Table 2.

Table 2. Comparison of key performance parameters between the SPNLC + LCPG and FLC + LCPG schemes.

Scheme	Test Wavelength	Response Time	Phase Modulation Type	Switching Voltage	Number of Components (Per Stage)	Alignment Layer Required
SPNLC + LCPG	405 nm	Sub-millisecond (~560 μs)	Continuous	~20–27 V	2	No
FLC + PG [14–16]	1064 nm	Microsecond (~100 μs)	Discrete	~5–10 V	4	Yes

These advantages make the proposed scheme promising for applications requiring large phase depth and continuous wavefront shaping, such as laser communications and adaptive optics. It should be noted that current 30 μm SPNLC devices have a transmittance of approximately 19.6 per cent at 405 nm, indicating that there is still considerable scope for reducing light scattering; meanwhile, 5 μm SPNLC devices have a transmittance of approximately 80 per cent at a wavelength of 650 nm, suggesting that appropriately reducing the cell thickness and increasing the operating wavelength are effective ways to improve transmittance. Consequently, future work will focus on the following areas: 1. Suppressing light scattering and enhancing system efficiency: This can be achieved by optimising fabrication process parameters (adjusting monomer concentration, polymerisation temperature and UV curing conditions), appropriately reducing the thickness of the liquid crystal cell and selecting material combinations with better refractive index matching, thereby further improving the device's transmittance. 2. Reducing the driving voltage: This can be achieved by optimising the morphology of the polymer network and reducing the thickness of the liquid crystal cell, amongst other measures. 3. Extending into the near-infrared and even long-wave infrared bands: As the scattering effects of SPNLCs will be significantly reduced at longer wavelengths, extending their operating wavelength into the near-infrared and even long-wave infrared bands is a direction worth exploring. 4. Exploring alternative material formulations: These include high-birefringence liquid crystal matrices, liquid crystal monomers with varying reactivity, and functionalised polymer networks, with a view to further enhancing the overall performance of the device.

5. Conclusions

We have proposed and demonstrated a fast non-mechanical beam deflector by cascading an SPNLC optical switch with LCPGs. A 30-μm-thick SPNLC electrically tunable half-wave plate is fabricated, which introduces a phase retardation of 3.6 μm within 300 V and achieves a sub-millisecond response time. Cascaded with passive LCPGs, fast electrically controlled switching of the beam between the ±1st diffraction orders is realized, and a two-dimensional multi-angle deflection module is constructed based on a supra-binary cascade scheme. The proposed approach maintains sub-millisecond response speed while providing continuous linear phase modulation capability and phase retardation up to several micrometers, with no need for an alignment layer, offering a technically viable pathway for high-performance non-mechanical beam steering with both fast response and fabrication simplicity.

Author Contributions: Conceptualization, J.C., L.X. and C.Z.; methodology, J.C., Z.C. and X.L.; validation, J.C., Z.C. and X.L.; resources, L.X.; writing—original draft preparation, J.C.; writing—review and editing, J.C.; supervision, L.X.; project administration, Y.W.; funding acquisition, L.X. and C.Z. All authors have read and agreed to the published version of the manuscript.

Funding: This research was funded by the Research Initiation Fund of Jiangsu University of Science and Technology (grant number 1052932208), Natural Science Foundation of Jiangsu Province (BK20251028), and the National Key Laboratory of Electromagnetic Space Security programs (grant numbers 2055082406 and 2055082501).

Institutional Review Board Statement: Not applicable.

Informed Consent Statement: Not applicable.

Data Availability Statement: The raw data supporting the conclusions of this article will be made available by the authors on request.

Conflicts of Interest: The authors declare no conflicts of interest.

References

1. McManamon, P.F.; Dorschner, T.A.; Corkum, D.L.; Friedman, L.J.; Hobbs, D.S.; Holz, M.; Liberman, S.; Nguyen, H.; Resler, D.; Sharp, R.; et al. Optical phased array technology. *Proc. IEEE* **1996**, *84*, 268–298. [CrossRef]
2. McManamon, P.F.; Bos, P.J.; Escuti, M.J.; Heikenfeld, J.; Serati, S.; Xie, H.; Watson, E.A. A review of phased array steering for narrow-band electrooptical systems. *Proc. IEEE* **2009**, *97*, 1078–1096. [CrossRef]
3. Naumov, A.; Love, G.; Loktev, M.Y.; Vladimirov, F. Control optimization of spherical modal liquid crystal lenses. *Opt. Express* **1999**, *4*, 344–352. [CrossRef] [PubMed]
4. Nersisyan, S.R.; Tabiryan, N.V.; Steeves, D.M.; Kimball, B.R. The promise of diffractive waveplates. *Opt. Photonics News* **2010**, *21*, 40–45. [CrossRef]
5. Jakeman, E.; Raynes, E. Electro-optic response times in liquid crystals. *Phys. Lett. A* **1972**, *39*, 69–70. [CrossRef]
6. Kawabe, K.; Furuhashi, T.; Tanaka, Y. (Eds.) 35.4: New TFT-LCD Driving Method For Improved Moving Picture Quality. In *SID Symposium Digest of Technical Papers*; Wiley: Hoboken, NJ, USA, 2001. [CrossRef]
7. Iwata, Y.; Murata, M.; Tanaka, K.; Jinda, A.; Ohtake, T.; Shinomiya, T.; Yoshida, H. (Eds.) 34.1: Novel super-fast-response, ultra-wide temperature range VA-LCD. In *SID Symposium Digest of Technical Papers*; Wiley: Hoboken, NJ, USA, 2013. [CrossRef]
8. Matsushima, T.; Okazaki, K.; Yang, Y.; Takizawa, K. (Eds.) 43.2: New fast response time in-plane switching liquid crystal mode. In *SID Symposium Digest of Technical Papers*; Wiley: Hoboken, NJ, USA, 2015. [CrossRef]
9. Fan, Y.-H.; Ren, H.; Liang, X.; Lin, Y.-H.; Wu, S.-T. Dual-frequency liquid crystal gels with submillisecond response time. *Appl. Phys. Lett.* **2004**, *85*, 2451–2453. [CrossRef]
10. Kowerdziej, R.; Wróbel, J.; Kula, P. Ultrafast electrical switching of nanostructured metadevice with dual-frequency liquid crystal. *Sci. Rep.* **2019**, *9*, 20367. [CrossRef] [PubMed]
11. Cattaneo, L.; Savoini, M.; Muševič, I.; Kimel, A.; Rasing, T. Ultrafast all-optical response of a nematic liquid crystal. *Opt. Express* **2015**, *23*, 14010–14017. [CrossRef] [PubMed]
12. Choi, H.; Higuchi, H.; Kikuchi, H. Fast electro-optic switching in liquid crystal blue phase II. *Appl. Phys. Lett.* **2011**, *98*, 131905. [CrossRef]
13. Xu, D.; Yan, J.; Yuan, J.; Peng, F.; Chen, Y.; Wu, S.-T. Electro-optic response of polymer-stabilized blue phase liquid crystals. *Appl. Phys. Lett.* **2014**, *105*, 011119. [CrossRef]
14. Guo, Q.; Xu, L.; Sun, J.; Yang, X.; Liu, H.; Yan, K.; Zhao, H.; Chigrinov, V.G.; Kwok, H.S. Fast switching beam steering based on ferroelectric liquid crystal phase shutter and polarisation grating. *Liq. Cryst.* **2019**, *46*, 1383–1388. [CrossRef]
15. Yuan, R.; Liu, Y.; Tan, Q.; Ge, J.; Chen, P.; Guo, Q.; Hu, W. An all-liquid-crystal strategy for fast orbital angular momentum encoding and optical vortex steering. *IEEE J. Sel. Top. Quantum Electron.* **2021**, *28*, 6000106. [CrossRef]
16. Yuan, F.; Tan, Q.; Wan, G.; Yuan, R.; Hu, W. Fast and large-angle optical beam deflection based on liquid crystal polarization grating. *Chin. J. Liq. Cryst. Disp.* **2022**, *37*, 1411–1419. [CrossRef]
17. West, J.L.; Zhang, G.; Glushchenko, A.; Reznikov, Y. Fast birefringent mode stressed liquid crystal. *Appl. Phys. Lett.* **2005**, *86*, 031111. [CrossRef]
18. Wang, B.; Zhang, G.; Glushchenko, A.; West, J.L.; Bos, P.J.; McManamon, P.F. Stressed liquid-crystal optical phased array for fast tip-tilt wavefront correction. *Appl. Opt.* **2005**, *44*, 7754–7759. [CrossRef] [PubMed]
19. Oh, C.; Escuti, M.J. Achromatic diffraction from polarization gratings with high efficiency. *Opt. Lett.* **2008**, *33*, 2287–2289. [CrossRef] [PubMed]
20. Kim, J.; Oh, C.; Escuti, M.J.; Serati, S. (Eds.) Wide-angle nonmechanical beam steering using thin liquid crystal polarization gratings. In *Advanced Wavefront Control: Methods, Devices, and Applications VI*; SPIE: Bellingham, WA, USA, 2008. [CrossRef]
21. Kim, J.; Miskiewicz, M.N.; Serati, S.; Escuti, M.J. (Eds.) Demonstration of large-angle nonmechanical laser beam steering based on LC polymer polarization gratings. In *Acquisition, Tracking, Pointing, and Laser Systems Technologies*; SPIE: Bellingham, WA, USA, 2011; Volume XXV. [CrossRef]
22. Attia, M.; Jonathan, J.M.C. Anisotropic gratings recorded from two circularly polarized coherent waves. *Opt. Commun.* **1983**, *47*, 85–90. [CrossRef]
23. Todorov, T.; Tomova, N.; Nikolova, L. High-sensitivity material with reversible photo-induced anisotropy. *Opt. Commun.* **1983**, *47*, 123–126. [CrossRef]
24. Ye, Y.-D.; Yan, H.; Wang, F.; Li, J.-M.; Li, G.-H.; Luo, Z.-X.; Hu, X.-Y. Phase compensation with rotating quarter waveplate in polarizing beam splitting scheme of laser launched and received in common aperture. *Qiangjiguang Yu Lizishu (High Power Laser Part. Beams)* **2006**, *18*, 749–752.

25. Muravsky, L.; Ostash, O.; Voronyak, T.; Andreiko, I. Two-frame phase-shifting interferometry for retrieval of smooth surface and its displacements. *Opt. Lasers Eng.* **2011**, *49*, 305–312. [CrossRef]
26. Khoo, I.-C.; Zhang, G.; Glushchenko, A.; West, J.L.; Smalyukh, I.; Lavrentovich, O. A model of stressed liquid crystals: Close-packed, shaped liquid crystal droplets inside a sheared polymer matrix. In *Liquid Crystals IX*; SPIE: Bellingham, WA, USA, 2005.

Disclaimer/Publisher's Note: The statements, opinions and data contained in all publications are solely those of the individual author(s) and contributor(s) and not of MDPI and/or the editor(s). MDPI and/or the editor(s) disclaim responsibility for any injury to people or property resulting from any ideas, methods, instructions or products referred to in the content.